Ultrafast Transfer and Transient Entrapment of Photoexcited Mg Electron in Mg@C_{60}

Mohamed El-Amine Madjet,[1,2,*] Esam Ali,[2] Marcelo Carignano,[3] Oriol Vendrell,[4] and Himadri S. Chakraborty[2,†]

[1]*Max-Planck-Institut für Physik komplexer Systeme, Nöthnitzer Straße 38, 01187 Dresden, Germany*
[2]*Department of Natural Sciences, D. L. Hubbard Center for Innovation, Northwest Missouri State University, Maryville, Missouri 64468, USA*
[3]*Department of Biomedical Engineering, Northwestern University, Evanston, Illinois 60208, USA*
[4]*Theoretical Chemistry, Institute of Physical Chemistry and Centre for Advanced Materials, Heidelberg University, Im Neuenheimer Feld 229 and 225, 69120 Heidelberg, Germany*

(Received 6 October 2020; revised 12 February 2021; accepted 26 March 2021; published 5 May 2021)

Electron relaxation is studied in endofullerene Mg@C_{60} after an initial localized photoexcitation in Mg by nonadiabatic molecular dynamics simulations. Two approaches to the electronic structure of the excited electronic states are used: (i) an independent particle approximation based on a density-functional theory description of molecular orbitals and (ii) a configuration-interaction description of the many-body effects. Both methods exhibit similar relaxation times, leading to an ultrafast decay and charge transfer from Mg to C_{60} within tens of femtoseconds. Method (i) further elicits a transient trap of the transferred electron that can delay the electron-hole recombination. Results shall motivate experiments to probe these ultrafast processes by two-photon transient absorption or photoelectron spectroscopy in gas phase, in solution, or as thin films.

DOI: 10.1103/PhysRevLett.126.183002

Synthesis, extraction, and isolation methods of endofullerenes with encapsulated atoms and molecules are fast developing [1,2]. Time domain spectroscopy of these stable, highly symmetric systems can test advances in laboratory techniques and access real time novel processes of fundamental and applied interest. Because of their exceptional properties, progression of technology piggybacks fullerene and endofullerene materials through applications in molecular devices [3,4], energy storage [5], and conversion [6,7].

Photoinduced charge transfer (CT) is a key process in organic photovoltaics whose donor-acceptor complexes are predominantly based on fullerene materials. This is because a fullerene molecule can be chemically tuned by choosing its endohedral core [8] or exohedral ligands including polymers [9,10] to control light absorption efficiency and carrier transport. Upon absorbing a photon, the energy converts to an exciton that either dissociates into free carriers or recombines depending on the electron-hole separation and excitonic binding energy. Of course, the dissociation is preferred for photovoltaics [11]. Thus, the decay and transfer of a "hot" electron from one location of the molecular material to another is a fundamental subprocess of this mechanism [12–16]. Therefore, gaining insights into the CT dynamics by addressing a simpler prototype system is very important.

These ultrafast processes occur on the femtoseconds to picoseconds timescale and are driven by the strong coupling between ionic and electronic degrees of freedom. Frameworks based on nonadiabatic molecular dynamics (NAMD), therefore, are appropriate for providing accurate, comprehensive descriptions of the processes [12,17]. Experimentally, ultrafast transient absorption spectroscopy (UTAS) [18–20] and time-resolved photoelectron spectroscopy (TRPES) [11,21] using femtosecond pulses or, more recently, attosecond pulses for greater resolution [22,23], can probe such dynamics in real time. Indeed, photoinduced charge migration has been measured in the time domain for fullerene-based polymerized films [15] and heterojunctions [16], and also for bulks [24] and nanorods [25]. However, these systems are large and, consequently, the relaxation pathways may intermix with concurrent processes that can wash out, mask, or camouflage spectral information on fundamental CT mechanisms, including access to prominent transient events.

From both theoretical and experimental standpoints, Mg@C_{60} serves as an excellent benchmark system to study the ultrafast relaxation and charge separation of an exciton in contact with an organic matrix. (i) It features a "surgical" photoexcitation at a local site. (ii) It showcases a pristine relaxation dynamics, consisting of the photoelectron's transfer to an entirely different site. (iii) Its dynamics upon photoexcitation proceeds through potentially long-lived intermediate states, similar to that in transient charge trappings [26]. Figure 1 delineates these points and displays the molecular orbital energies of Mg@C_{60} based on a density-functional theory (DFT) description in Fig. 1(a). Figure 1(b) also includes the contour map of the transient

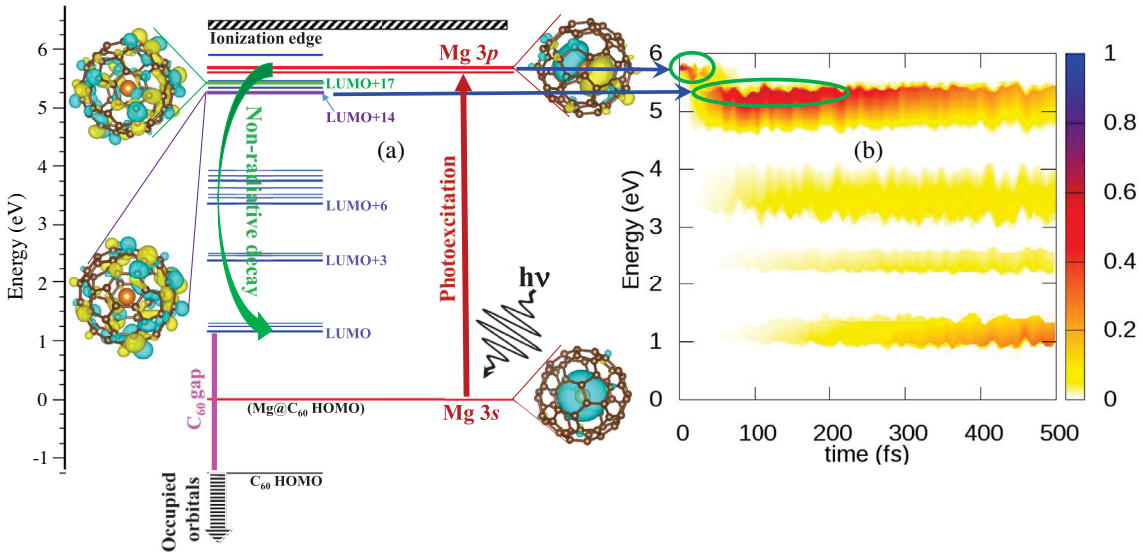

FIG. 1. (a) $Mg@C_{60}$ molecular orbital energies (relative to $Mg@C_{60}$ HOMO) at the DFT/B3LYP level of theory (see text). The Mg $3s \rightarrow 3p$ photoexcitation and subsequent CT decay are illustrated. Isosurface plots of Mg $3s$, LUMO+20 (Mg $3p$ type), LUMO+17, and LUMO+14 are shown. (b) Transient electronic state population dynamics following photoexcitation to LUMO+20 for the same simulations; initial excited population decay and transient capture in LUMO+14 are especially marked. The oscillations in time seen correspond to the vibrational motion on the ground state potential energy surface superimposed with the electronic dynamics.

excited electronic state population dynamics obtained from the DFT trajectories in our simulations. Notice how the valence Mg $3s$ level occurs isolated within the C_{60} band gap and thus can be conveniently excited by a UV pump pulse to Mg $3p$, corresponding to the degenerate orbitals LUMO+19 − LUMO+21, each retaining predominant Mg character (Fig. 2). This threefold degeneracy of the p states in totally symmetric geometries of the complex is lifted due to the symmetry-breaking interaction with C_{60}. These excited states, localized on Mg, are the initial states of our simulation. Nonradiative decay, driven by electron-phonon couplings, then becomes the dominant decay process; no intercoulombic decay channel [27,28] exists, since the Mg excitation energy is lower than the C_{60} ionization energy. This ultrafast relaxation is the subject of our simulations and can be followed by a time-delayed probe pulse in UTAS or TRPES, producing spectrographs [11,19–21] (in energies and delays) directly comparable to the time-dependent population map in Fig. 1(b). As the photoexcited electron decays to LUMO+17, the first pure C_{60} state (Fig. 1), an atom-to-C_{60} CT occurs. This CT is complete and irreversible and thus offers a clean, well-defined event for experimental measurements. Decaying further, the electron lands on LUMO+14 and experiences a transient hold-up due to a wide energy gap below this state that hinders the subsequent decay. Consequently, the lifetime of the LUMO+14 population is predicted to be longer than for nearby states. Even though there are gaps below LUMO+6 and LUMO+3, their peak populations never grow enough, as seen in Fig. 1, due to significant slowdown.

We consider first the simulations performed with an independent particle (IP), molecular orbital description of the electrons in the DFT frame using the B3LYP exchange-correlation functional (see Supplemental Material [29]). The computed molecular orbitals ϕ_j and energies ϵ_j along

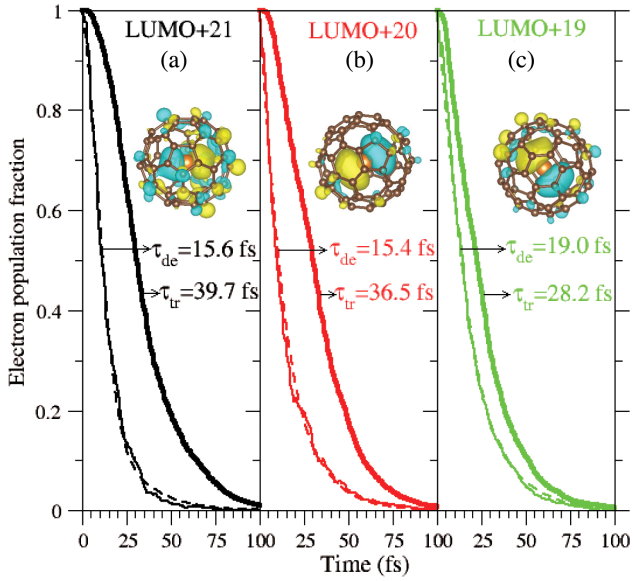

FIG. 2. Time evolutions of the decay and transfer population fractions after three initial excitations to (a) LUMO+21, (b) LUMO+20, and (c) LUMO+19, corresponding to Mg $3p$ threefold degenerate orbitals. The decay (τ_{de}) and transfer (τ_{tr}) times shown are extracted by curve fittings (see text) and the fit curves for the decay are shown by the dashed lines.

the nuclei trajectories are used to obtain electron-phonon nonadiabatic couplings (NACs) d_{jk} [47],

$$d_{jk} = \frac{\langle \phi_j | \vec{\nabla}_R H | \phi_k \rangle}{\epsilon_k - \epsilon_j} \frac{\partial \vec{R}}{\partial t}, \quad (1)$$

where H and $\vec{R}$ are the electronic Hamiltonian and nuclear coordinate. Evidently, NACs can enhance by (i) larger orbital overlaps, (ii) narrower energy separations, and (iii) faster nuclear velocities.

The NAMD simulations of the dynamics of Mg@C_{60} start from a localized excitation of Mg 3s to each of the 3p states, LUMO+21, LUMO+20, and LUMP+19. Figure 2 presents the time evolution of the relaxations. From the initial excited state, the hot electron quickly spreads to the other two states of the 3p degeneracy owing to their strong NACs from large orbital overlaps [Eq. (1)] before the electron transfers to lower states. The time evolution of the population fractions of the initial states are plotted in Fig. 2. Their decay times (τ_{de}) are evaluated by fitting to the sum of an exponential and a Gaussian decay function, as 15.6, 15.4, and 19.0 fs, respectively. The small time differences are caused by the lowered symmetry of the initial conditions compared with the totally symmetric geometry of the complex and can be seen as a statistical spread of the decay time when populating the Mg p levels. τ_{de} for LUMO+19 is slightly longer because some excited population to LUMO+20 and LUMO+21 repopulates LUMO+19 back, highlighting the role of the nuclear-driven electronic dynamics within the quasidegenerate window of 3p states.

While LUMO+17 is found to be the first dominant C_{60} state on the decay path, LUMO+18 is an atom-C_{60} hybrid state. Thus, in order to estimate the atom-to-C_{60} electron transfer time (τ_{tr}) from a given initial excited state, we add up the population of the three 3p states and half of that of hybrid LUMO+18. The resultant cumulative curves, representing the transfer dynamics, are also included in Fig. 2. Fittings yield the values of τ_{tr} to be 39.7, 36.5, and 28.2 fs, respectively. The slower transfer trend going from the higher to lower initial state points to the fact that the higher the excitation the longer the electron takes to evacuate the Mg region. The signature of this decay can be observed in the map of Fig. 1(b). Further, one may visualize the original electron-hole pair in Mg as a *local* exciton, while the exciton after the electron transfers to the cage with a hole at Mg 3s is a *nonlocal* exciton. Therefore, τ_{tr} also corresponds to the ultrafast conversion time from a local to a nonlocal exciton, leading to the generation of carriers. Vibronic coupling suppresses the electron-hole recombination owing to energy dissipation to the vibrational modes of C_{60}. In solid C_{60}, the exciton biding energy has a large value ~0.5 eV [48], which disfavors their separation to free charges.

The state LUMO+14 acts as a transient trapper for the electron. Indeed, based on Eq. (1), the population of LUMO+14 grows at a higher rate fed by energetically close states above it (Fig. 1), while the energy gap below LUMO+14 leads to a slower depopulation. Figure 3 shows the net electron population dynamics of LUMO+14 for each initial Mg excitation. The peak of LUMO+14 rises to about 65% of the population; hence this transient population can likely be experimentally accessed. A sum of exponential and Gaussian growth *plus* decay functions are used to fit the curves to extract the trapping times (τ) of 202, 227, and 230 fs, respectively. Again, the electron resides slightly longer in the atomic site when excited to a higher state. This fact is reflected by earlier time (t_{max}) of 88 fs at which the maximum population of LUMO+14 is reached when the electron was initially excited to LUMO+19. As already mentioned, these time spreads arise from the statistical uncertainty of the initial conditions, in which the degeneracy of the p levels has been lifted along the nuclear trajectories. Only after 100 fs the LUMO starts to gain population and reaches about 30% at 500 fs. This significant slowdown at the band edge is due to additional slowing effects induced by the gaps below LUMO+6 and LUMO+3. However, like the population

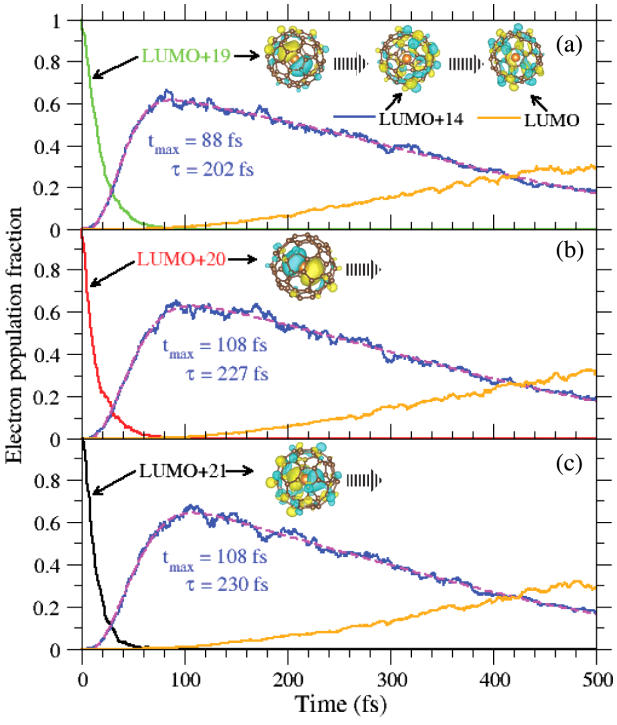

FIG. 3. Time evolutions of the population fractions of the trapper state LUMO+14 and the band edge LUMO after initial excitations to (a) LUMO+19, (b) LUMO+20, and (c) LUMO+21. The excited state decays are also shown. The lifetime (τ) and the time (t_{max}) of maximum population of LUMO+14 are extracted by curve fittings; the fit curves are shown as the dashed lines.

peak of LUMO, that of LUMO+6 and LUMO+3 are so low that it will likely be difficult to measure them. We note that such intermittent gaps in C_{60} unoccupied levels were found in other calculations [36]. Thus, within the reliability of the B3LYP functional, the prediction of a strong population trap atop the first gap on the decay path appears to be plausible. The fact that all these dynamics are reasonably captured as population growth and decay traces in Fig. 1(b) bodes well for UTAS and/or TRPES measurements in probing the dominant effects.

The computation scheme used above in the IP framework neglected the electron-electron and electron-hole interactions. To account for the many-electron effects, we now apply a configuration-interaction singles (CIS) approach (see Supplemental Material [29]). For the optimized structure, the excitation of Mg corresponds to an energy of 4.95 eV and has an oscillator strength of ~0.15 (allowed transition). The corresponding excited state is threefold degenerate, as expected, with energies close to the $3s \rightarrow$ LUMO+21, LUMO+20, LUMO+19 excitations in the IP treatment, and corresponds to the CIS excited states: S_{34}, S_{35}, and S_{36}. Figure 4 shows the electron density difference, excited minus ground, for S_{36} and S_{34} at $t = 0$, where their localized Mg nature can be seen; the golden color encodes positive values, while the green is negative. The central negative lobes are due to the subtraction of the ground Mg $3s$ spherical density.

After the initial ($t = 0$) excitation of Mg, as illustrated in Fig. 4 for S_{36} in a NAMD trajectory, the electron population follows structural rearrangements driven nonadiabatically by the electron-phonon couplings. After 35.5 fs, S_{36} decays to S_{21} to complete the electron transfer to C_{60}. This is

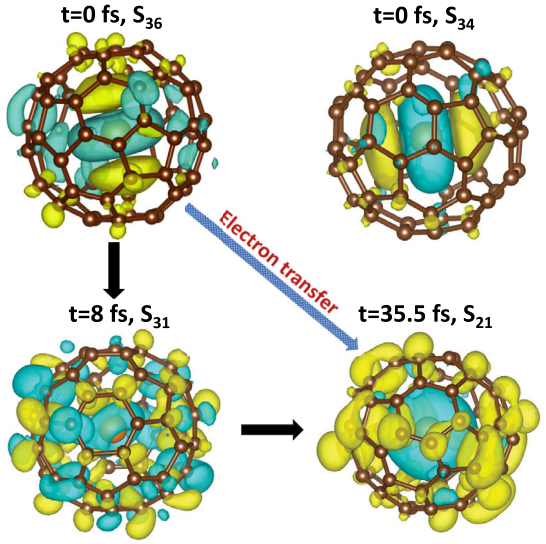

FIG. 4. Electron density difference (excited *minus* ground) of $Mg@C_{60}$ with isodensity value of ±0.0005 a.u. with positive (golden) and negative (green) values. Results at $t = 0$ for S_{36} and S_{34}, and the electron transfer for S_{36} in a molecular dynamics trajectory, are shown.

evident in the isodensity plot of S_{21} where the negative values are localized on Mg and the positive values are on the cage. Note also the plot at an intermediate time of 8 fs, which denotes a hybrid state. The 35.5-fs transfer time is close to the average of the three values of τ_{tr} in Fig. 2, suggesting that the many-body dynamics, which dominates the plasmon-driven ionization spectra [49] at higher energies (XUV), is not critical in the middle UV region of current interest. Furthermore, most of the excited states below S_{34} are found to be dark—a fact that favors a localized photoexcitation of Mg—and are only populated during the relaxation of the hot electron.

Similar to our IP model, there are energy gaps between CIS excited states below S_{21}. These gaps (~0.3 eV) are not large enough to result in a transient capture of the excited population, which now continues to relax toward lower-energy states. A reason for such denser CIS spectrum is the presence of satellite states originating from linear combinations of coupled particle-hole configurations. However, whether this higher density of states necessarily quenches the trapping mechanism observed in the IP model remains an open question. The current study combines CIS trajectories with a Landau-Zener (LZ) scheme (see Supplemental Material [29]) to calculate the hopping probability. But it is conceivable that some of the NACs computed via Eq. (1) (using electronic states instead of orbitals) would be smaller than the LZ prediction [two states may feature a small energy gap, yet the numerator in Eq. (1) may be small or even vanish]. However, the evaluation of accurate NACs for correlated states in this large system is currently out of reach. In order to draw a more fair comparison, one also needs to perform B3LYP/time dependent DFT calculations, besides Hartree-Fock/CIS, to bring the correlated calculations to same footing as the IP method. On the other hand, the excellent match between the CT times by both methods suggests that many-electron effects may be weak at the onset of relaxation, which is determined instead by electron-vibration coupling. The differences found in the subsequent dynamics, as to whether a transient trapping of the electronic population might be present, offer a unique motivation to conduct experiments and extend calculations in endofullerenes.

For the experiment, $Mg@C_{60}$ can be synthesized by the ion implantation technique in a similar manner employed for $Li@C_{60}$ [50], which showed stability in the air after sublimation [51]. The ion energy can be optimized to allow the encapsulation and yet to minimize the destruction of fullerenes, so $Mg@C_{60}$ can be isolated from the collision debris. The air stability of $Mg@C_{60}$ might be a challenge owing to the oxidation state $Mg^{2+}@C_{60}^{2-}$, but this could be mitigated by converting to a stable salt form with $Mg^{2+}@C_{60}$ cation and some stabilizing anion, as was accomplished for $Li@C_{60}$ [52]. For example, $Ca@C_{60}$ was produced with a laser vaporization source and its photoelectron spectroscopy in gas phase was performed [53].

Because of the noncovalent interactions of $Mg@C_{60}$ with its environment, we believe that the essence of our results will remain valid under such modifications and also in solution or in thin films.

To conclude, we simulated and analyzed the ultrafast nonradiative relaxation process, driven by electron-phonon coupling (lattice thermalization), of a photoexcited electron in an atom confined in C_{60}. $Mg@C_{60}$ presents a clean and uncluttered electron relaxation to the outer C_{60} shell, possibly featuring a transient slowdown of the electron relaxation process in real time due to the presence of large gaps in the spectrum of excited electronic states. The possibility of inducing the initial excitation accurately within Mg makes this molecule an ideal example for ultrafast transient absorption or photoelectron spectroscopic studies. Good agreement at early times between the two employed methods, with and without the many-body interactions, indicates that the ultrafast charge separation of the initial exciton with tens of femtoseconds driven by vibronic effects is a robust result. The study provides a reference to understand both experimental and theoretical investigations on endofullerene derivatives with increasing structural complications via functionalization and we hope that the current research will motivate experimental activities in the domain of ultrafast science.

Computing time at Bartik High-Performance Cluster (National Science Foundation Grant No. CNS-1624416, U.S.) in Northwest Missouri State University is acknowledged. Dr. Felipe Zapata is acknowledged for help and assistance with QMflows code. We thank Dr. Alexey Popov and Dr. Eleanor Campbell for encouraging discussions on synthesis possibilities of $Mg@C_{60}$ for future experiments. The research is supported by the National Science Foundation Grant No. PHY-1806206, U.S.

*mmadjet@pks.mpg.de
†himadri@nwmissouri.edu

[1] A. A. Popov, Synthesis and molecular structures of endohedral fullerenes, in *Endohedral Fullerenes: Electron Transfer and Spin*, Nanostructure Science and Technology Series, edited by A. A. Popov (Springer, Cham, 2017).

[2] F. Liu, J. Guan, T. Wei, S. Wang, and S. Yang, Chapter 2: Synthesis and isolation of endohedral fullerenes a general review, *Endohedral Fullerenes: From Fundamentals to Applications*, edited by S. Yang and C.-R. Wang (World Scientific, Singapore, 2014).

[3] H. J. Chandler, M. Stefanou, E. E. B. Campbell, and Renald Schaub, $Li@C_{60}$ as a multi-state molecular switch, Nat. Commun. **10**, 2283 (2019).

[4] Y. Chai, X. Liu, B. Wu, L. Liu, Z. Wang, Y Weng, and C. Wang, In Situ switching of photoinduced electron transfer direction by regulating the redox state in fullerene-based dyads, J. Am. Chem. Soc. **142**, 4411 (2020).

[5] J. Friedl, M. A. Lebedeva, K. Porfyrakis, U. Stimming, and T. W. Chamberlain, All-fullerene-based cells for nonaqueous redox flow batteries, J. Am. Chem. Soc. **140**, 401 (2018).

[6] I. Jeon, A. Shawky, H.-S. Lin, S. Seo, H. Okada, J.-W. Lee, A. Pal, S. Tan, A. Anisimov, E. I. Kauppinen, Y. Yang, S. Manzhos, S. Maruyama, and Y. Matsuo, Controlled redox of lithium-ion endohedral fullerene for efficient and stable metal electrode-free perovskite solar cells, J. Am. Chem. Soc. **141**, 16553 (2019).

[7] S. Collavini and J. L. Delgado, Fullerenes: The stars of photovoltaics, Sustainable Energy Fuels **2**, 2480 (2018).

[8] R. B Ross, C. M Cardona, D. M Guldi, S. G. Sankaranarayanan, M. O. Reese, N. Kopidakis, J. Peet, B. Walker, G. C. Bazan, E. Van Keuren, B. C. Holloway, and M. Drees, Endohedral fullerenes for organic photovoltaic devices, Nat. Mater. **8**, 208 (2009).

[9] Y. J. He and Y. F. Li, Fullerene derivative acceptors for high performance polymer solar cells, Phys. Chem. Chem. Phys. **13**, 1970 (2011).

[10] C.-Z. Li, H.-L. Yipab, and A. K.-Y. Jen, Functional fullerenes for organic photovoltaics, J. Mater. Chem. **22**, 4161 (2012).

[11] S. Emmerich, S. Hedwig, M. Cinchetti, B. Stadtmüller, and M. Aeschlimann, Ultrafast charge carrier separation in potassium-intercalated endohedral metallofullerene $Sc_3N@C_{80}$ thin films, arXiv:2002.04576.

[12] K. Sato, E. Pradhan, R. Asahia, and A. V. Akimov, Charge transfer dynamics at the boron subphthalocyanine chloride/C_{60} interface: Non-adiabatic dynamics study with Libra-X, Phys. Chem. Chem. Phys. **20**, 25275 (2018).

[13] M. Ortiz, S. Cho, J. Niklas, S. Kim, O. G. Poluektov, W. Zhang, G. Rumbles, and J. Park, Through-space ultrafast photoinduced electron transfer dynamics of a C_{70}-encapsulated bisporphyrin covalent organic polyhedron in a low-dielectric medium, J. Am. Chem. Soc. **139**, 4286 (2017).

[14] G. Boschetto, M. Krompiec, and C.-K. Skylaris, Insights into the charge-transfer mechanism of organic photovoltaics: Effect of domain size, J. Phys. Chem. C **122**, 17024 (2018).

[15] F. Juvenal, H. Lei, A. Schlachter, P.-L. Karsenti, and P. D. Harvey, Ultrafast photoinduced electron transfers in Platinum(II)- anthraquinone diimine polymer/PCBM films, J. Phys. Chem. C **123**, 5289 (2019).

[16] C.-H. Cheng, B.-L. Zhang, H.-Q. Song, Y. Wang, W.-H. Li, J. Liu, J. Leng, W. Tian, C. Zhao, S. Jin, W. Liu, and S. Cong, Photoinduced ultrafast electron transfer and charge transport in a PbI_2/C_{60} heterojunction, J. Phys. Chem. C **123**, 30791 (2019).

[17] T. R. Nelson, A. J. White, J. A. Bjorgaard, A. E. Sifain, Y. Zhang, B. Nebgen, S. Fernandez-Alberti, D. Mozyrsky, A. E. Roitberg, and S. Tretiak, Non-adiabatic excited-state molecular dynamics: Theory and applications for modeling photophysics in extended molecular materials, Chem. Rev. **120**, 2215 (2020).

[18] R. Berera, R. van Grondelle, and J. T. M. Kennis, Ultrafast transient absorption spectroscopy: Principles and application to photosynthetic systems, Photosynth. Res. **101**, 105 (2009).

[19] A. Bhattacherjee, C. D. Pemmaraju, K. Schnorr, A. R. Attar, and S. R. Leone, Ultrafast intersystem crossing in

acetylacetone via femtosecond x-ray transient absorption at the carbon K-edge, J. Am. Chem. Soc. **139**, 16576 (2017).
[20] F. Gesuele, Ultrafast hyperspectral transient absorption spectroscopy: Application to single layer graphene, Photonics **6**, 95 (2019).
[21] B. Stadtmüller, S. Emmerich, D. Jungkenn, N. Haag, M. Rollinger, S. Eich, M. Maniraj, M. Aeschlimann, M. Cinchetti, and S. Mathias, Strong modification of the transport level alignment in organic materials after optical excitation, Nat. Commun. **10**, 1470 (2019).
[22] T. Driver *et al.*, Attosecond transient absorption spooktroscopy: A ghost imaging approach to ultrafast absorption spectroscopy, Phys. Chem. Chem. Phys. **22**, 2704 (2020).
[23] R. Geneaux, H. J. B. Marroux, A. Guggenmos, D. M. Neumark, and S. R. Leone, Transient absorption spectroscopy using high harmonic generation: A review of ultrafast x-ray dynamics in molecules and solids, Phil. Trans. R. Soc. A **377**, 20170463 (2019).
[24] J. He, L. Zhang, D. He, Y. Wang, Z. He, and H. Zhao, Ultrafast transient absorption measurements of photocarrier dynamics in monolayer and bulk $ReSe_2$, Opt Express **26**, 21501 (2018).
[25] G. Kedawat, I. Sharma, K. Nagpal, M. Kumar, Govind Gupta, and B. K. Gupta, Studies of ultrafast transient absorption spectroscopy of gold nanorods in an aqueous solution, ACS Omega **4**, 12626 (2019).
[26] C. R. Carey, Y. Yu, M. Kuno, and G. V. Hartland, Ultrafast transient absorption measurements of charge carrier dynamics in single II-VI nanowires, J. Phys. Chem. C **113**, 19077 (2009).
[27] R. Obaid, H. Xiong, S. Augustin, K. Schnorr, U. Ablikim, A. Battistoni, T. J. A. Wolf, R. C. Bilodeau, T. Osipov, K. Gokhberg, D. Rolles, A. C. LaForge, and N. Berrah, Intermolecular Coulombic Decay in Endohedral Fullerene at the $4d \rightarrow 4f$ Resonance, Phys. Rev. Lett. **124**, 113002 (2020).
[28] M. H. Javani, J. B. Wise, R. De, Me. E. Madjet, S. T. Manson, and H. S. Chakraborty, Resonant auger-intersite-Coulombic hybridized decay in the photoionization of endohedral fullerenes, Phys. Rev. A **89**, 063420 (2014).
[29] See Supplemental Material at http://link.aps.org/supplemental/10.1103/PhysRevLett.126.183002 for details of the methodologies, under Method I and Method II, which includes Refs. [30–46].
[30] M. W. Schmidt, K. K. Baldridge, J. A. Boatz, S. T. Elbert, M. S. Gordon, J. H. Jensen, S. Koseki, N. Matsunaga, K. A. Nguyen, S. Su, T. L. Windus, M. Dupuis, and J. A. Montgomery, Jr., General atomic and molecular electronic structure system, J. Comput. Chem. **14**, 1347 (1993).
[31] M. S. Gordon and W. S. Michael, *Advances in Electronic Structure Theory: GAMESS a Decade Later* (Elsevier, Amsterdam, 2005), pp. 1167–1189.
[32] Vinit and C. N. Ramachandran, Structure, stability, and properties of boron encapsulated complexes of C_{60}, $C_{59}B$, and $C_{59}N$, J. Phys. Chem. A **121**, 1708 (2017).
[33] C.-R. Zhang, J. S. Sears, B. Yang, S. G. Aziz, V. Coropceanu, and J.-L. Brédas, Theoretical study of the local and charge-transfer excitations in model complexes of pentacene-C_{60} using tuned range-separated hybrid functionals, J. Chem. Theory Comput. **10**, 2379 (2014).
[34] D. Muigg, P. Scheier, K. Becker, and T. D. Märk, Measured appearance energies of C_n^+ $(3 \leq n \leq 10)$ fragment ions produced by electron impact on C_{60}, J. Phys. B **29**, 5193 (1996).
[35] D.-L. Huang, P. D. Dau, H.-T. Liu, and L.-S. Wang, High-resolution photoelectron imaging of cold C_{60}^- anions and accurate determination of the electron affinity of C_{60}, J. Chem. Phys. **140**, 224315 (2014).
[36] M. W. Schmidt, E. A. Hull, and T. L. Windus, Valence virtual orbitals: An unambiguous ab initio quantification of the LUMO concept, J. Phys. Chem. A **119**, 10408 (2015).
[37] J. Hutter, M. Iannuzzi, F. Schiffmann, and J. VandeVondele, CP2K: Atomistic simulations of condensed matter systems, Comput. Mol. Sci. **4**, 15 (2014).
[38] S. Grimme, Semiempirical GGA-type density functional constructed with a long-range dispersion correction, J. Comput. Chem. **27**, 1787 (2006).
[39] S. Grimme, J. Antony, S. Ehrlich, and H. Krieg, A consistent and accurate ab initio parametrization of density functional dispersion correction (DFT-D) for the 94 elements H-Pu, J. Chem. Phys. **132**, 154104 (2010).
[40] F. Zapata, L. Ridder, J. Hidding, C. R. Jacob, I. Infante, and L. Visscher, QMflows: A toll kit for interoperable parallel workflows in quantum chemistry, J. Chem. Inf. Model. **59**, 3191 (2019).
[41] A. V. Akimov and O. V. Prezhdo, The PYXAID program for non-adiabatic molecular dynamics in condensed matter systems, J. Chem. Theory Comput. **9**, 4959 (2013).
[42] A. V. Akimov and O. V. Prezhdo, Advanced capabilities of the PYXAID program: Integration schemes, decoherence effects, multiexcitonic states, and field-matter interaction, J. Chem. Theory Comput. **10**, 789 (2014).
[43] M. E. Madjet, A. V. Akimov, F. El-Mellouhi, G. R. Berdiyorov, S. Ashhab, N. Tabeta, and S. Kais, Enhancing the carrier thermalization time in organometallic perovskites by halide mixing, Phys. Chem. Chem. Phys. **18**, 5219 (2016).
[44] M. E. Madjet, G. R. Berdiyorov, F. El-Mellouhi, F. H. Alharbi, A. V. Akimov, and S. Kais, Cation effect on hot carrier cooling in halide perovskite materials, J. Phys. Chem. Lett. **8**, 4439 (2017).
[45] M. E. Madjet, Z. Li, and O. Vendrell, Ultrafast hydrogen migration in acetylene cation driven by non-adiabatic effects, J. Chem. Phys. **138**, 094311 (2013).
[46] W. J. Stevens, H. Basch, and M. Kraus, Compact effective potentials and efficient shared-exponent basis sets for the first- and second-row atoms, J. Chem. Phys. **81**, 6026 (1984).
[47] H. Guo, C. Zhao, Q. Zheng, Z. Lan, O. V. Prezhdo, W. A. Saidi, and J. Zhao, Superatom molecular orbital as an interfacial charge separation state, J. Phys. Chem. Lett. **9**, 3485 (2018).
[48] M. S. Golden, M. Knupfer, J. Fink, J. F. Armbruster, T. R. Cummins, H. A. Romberg, M. Roth, M. Sing, M. Schmidt, and E. Sohmen, The electronic structure of fullerenes and fullerene compounds from high-energy spectroscopy, J. Phys. Condens. Matter **7**, 8219 (1995).
[49] H. S. Chakraborty, M. E. Madjet, J.-M. Rost, and S. T. Manson, Dynamical effects of confinement on atomic valence photoionization of $Mg@C_{60}$, Phys. Rev. A **78**, 013201 (2008).

[50] C. Y. Lee, Ti^+ and Mg^+ Ion beam extraction from the modified bernas ion source, J. Korean Phys. Soc. **76**, 638 (2020).

[51] E. E. B. Campbell, R. Tellgmann, N. Krawez, and I. V. Hertel, Production and LDMS characterization of endohedral alkali-fullerene films, J. Phys. Chem Solids **58**, 1763 (1997).

[52] S. Aoyagi *et al.*, A layered ionic crystal of polar $Li@C_{60}$ superatoms, Nat. Chem. **2**, 678 (2010).

[53] L. S. Wang, J. M. Alford, Y. Chai, M. Diener, J. Zhang, S. M. McClure, T. Guo, G. E. Scuseria, and R. E. Smalley, The electronic structure of $Ca@C_{60}$, Chem. Phys. Lett. **207**, 354 (1993).